Vector field path following and obstacle avoidance singularity mitigation via look-ahead flight envelope

First A. Author* and Second B. Author Jr.†
Business or Academic Affiliation 1, City, State, Zip Code

Unmanned Aerial Vehicles conventionally navigate by following a series of pre-planned waypoints that may have to be re-planned when flying in a dynamic environment or encountering previously unknown obstacles. Waypoints are generally planned off-line and relayed to the UAV, taking up time and autopilot communication resources. Attractive path following and repulsive obstacle avoidance vector fields have been summed together to produce UAV guidance that follows pre-planned paths and avoids obstacles without the need to re-plan. Summing attractive and repulsive vector fields may produce small regions of null guidance, called singularities, which could potentially lead to trap situations. An investigation into singularity mitigation by vector field weight parameterization is presented.

I. Nomenclature

UAV = Unmanned Aerial Vehicle
VF = Vector Field
VFF = Virtual Force Field
LVF = Lyapunov Vector Field
GVF = Goncalves Vector Field

II. Introduction

Unmanned Aerial Vehicles (UAV)s are pilotless aircraft used by military, police, and civilian communities for tasks such as reconnaissance, damage assessment, surveying, and target tracking [1, 2]. Tasks can be performed by a single UAV or cooperate with a team of other air, ground, or marine vehicles [3–5]. UAVs are ideal for remote data collection due to their low cost, endurance, and reduced risk to human life. Data can be collected by loitering the aircraft around an area of interest (AOI) or along a sensor path, such as a road or tree-line. Missions for collecting data are typically pre-planned on a remote ground station where an obstacle free and flyable path is generated. Typically paths are deconstructed into a series of discrete waypoints that the UAV navigates to through the use of a line-of-sight guidance. While navigating the pre-planned path previously unknown obstacles may be discovered and a new obstacle free path may have to be generated, which may be difficult or impossible if the UAV is out of radio range. Additional methods for avoiding obstacles in real time include potential field and vector field which employ the use of artificial attractive and repulsive forces to pull a UAV towards a goal while pushing away from obstacles. Potential field is a popular solution to both path planning and guidance problems in obstacle rich environments, however suffers from several limitations including local minima, oscillations, and may cause excess deviation from the desired sensor line. Vector field guidance converges and circulates a pre-defined path and may be summed with additional repulsive vector fields to produce an obstacle avoidance. Previous methods only considered repulsive fields which do not aid in circumnavigating an obstacle and also introduce conditions which may lead to vector field singularities.

Further optimization of vector fields to include circulation may produce an efficient real-time guidance for avoiding obstacles while also removing singularities from the UAVs path. A method for determining obstacle decay radius, circulation, and repulsion such that a UAV avoids obstacles while minimizing path deviation is presented. The modified guidance will then be compared against waypoint, Potential Field, and un-modified path following guidance in simulation

*Insert Job Title, Department Name, Address/Mail Stop, and AIAA Member Grade (if any) for first author.
†Insert Job Title, Department Name, Address/Mail Stop, and AIAA Member Grade (if any) for second author.

for cross track error and deviation from sensor path. Lastly, the optimized vector field will then be demonstrated on a crazyflie 2.0 multi-rotor simulating fixed wing constraints.

A. Dubins Vehicle

UAVs traveling at constant altitude and speed u and with a limited turn rate $\dot{\theta}$ can be simplified as a Dubin's vehicle that flies in straight lines and circular arcs. The position of the UAV $\overrightarrow{X}$ at time t is calculated from the integral of the velocity vector $\overrightarrow{U}$. Heading is an input from a guidance system, such as waypoint, potential field, or vector field.

$$\overrightarrow{U}(t) = u \begin{bmatrix} cos(\theta(t)) \\ sin(\theta(t)) \end{bmatrix} \tag{1}$$

$$\overrightarrow{X}(t) = \overrightarrow{U} dt + \overrightarrow{X}(t-1) \tag{2}$$

$$\dot{\theta} \leq 20 deg/s \tag{3}$$

B. Optimal Path

A path for avoiding a circular obstacle while maximizing the sensor path coverage can be accomplished with three circular arc turns. The circular obstacle is defined to have a radius R and a lateral distance Y_0 from the sensor path in frame I. The first and third arc utilize the UAVs minimum turning radius, θ_r, calculated in Equation 4. The start of the first minimum radius turn begins when the UAV's horizontal position x reaches $\tilde{x}$ from the path frame. At a horizontal position $-\hat{x}$ the UAV turns with a radius of the obstacle R and exits when the UAVs horizontal position reaches $\hat{x}$.

$$\theta_r = \frac{u}{\dot{\theta}} \tag{4}$$

The horizontal points $\tilde{x}$ and $\hat{x}$ are shown in Equations 5 and 6 respectively.

$$\widetilde{x} = -\sqrt{(\theta_r + R)^2 - (\theta_r - Y_o)^2} \tag{5}$$

$$\hat{x} = \frac{R\sqrt{(r+R)^2 - (\theta_r - Y_o)^2}}{R + \theta_r} \tag{6}$$

The avoidance path for navigating around a circular obstacle with maximum coverage of a sensor line is defined in Equation 7 and shown in Figure 1.

$$y(x) = \begin{cases} \widetilde{y} - \sqrt{\theta_r^2 - (x - \widetilde{x})^2} & x < -\hat{x} \\ Y_o + \sqrt{R^2 - x^2} & -\hat{x} \leq x \geq \hat{x} \\ \widetilde{y} - \sqrt{\theta_r^2 - (x + \widetilde{x})^2} & x > -\hat{x} \end{cases} \tag{7}$$

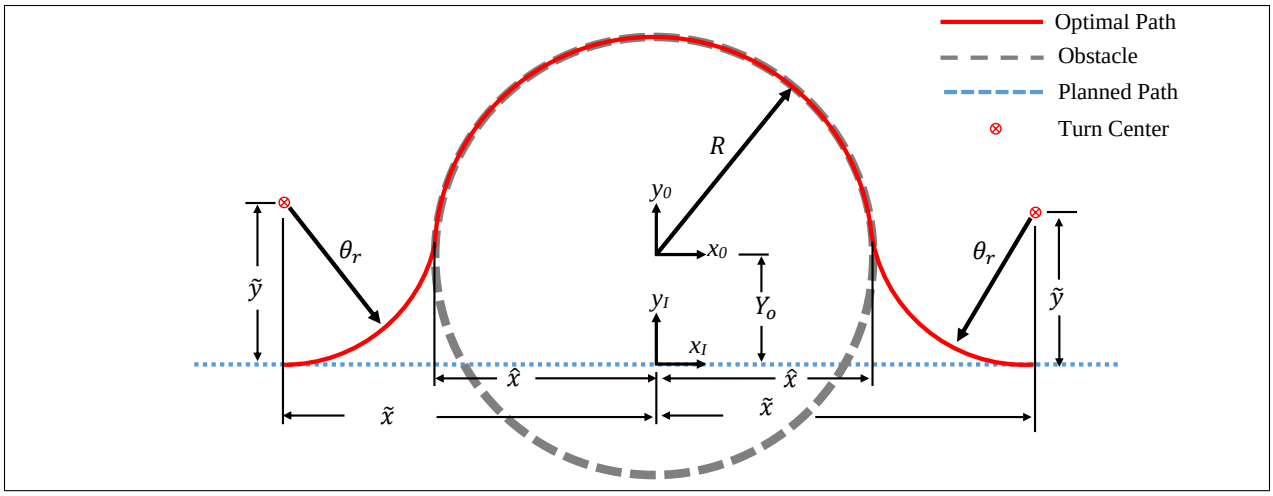

Fig. 1 Optimal Kinematic Path Around Circular Obstacle

The avoidance path represents the optimal path around a circular obstacle and would be used to generate waypoints for waypoint guidance.

C. Waypoint Guidance

Waypoint guidance aligns the vehicle with the currently active waypoint that lies along a pre-planned path. Paths are typically generated off-line and can be optimized for shortest distance traveled and further refined to be flyable for a particular vehicle. Paths may also be optimized to produce flight patterns that increase sensor coverage of an area of interest [6]. If an obstacle lies along that sensor path, the UAV must avoid the obstacle but also return back to the sensor path such that a minimal length of the path is missed during data collection. Waypoints placed on the outside the radius of the obstacle can direct a UAV around an obstacle and back onto the desired sensor path. Obstacles discovered during flight that lie along the pre-planned path may require a new path to be planned, requiring communication with the ground station. If a new path is not relayed to the UAV in time the vehicle may fail to avoid the obstacle. Waypoint navigation may not provide the most efficient path for avoiding an obstacle due to the waypoint radii, even if the path was determined from an optimal path planner. The waypoints would most likely be placed outside of the obstacle's edge to keep the waypoint's detection radius outside of the obstacle region. An example of waypoints planned around an obstacle is shown in Figure 2 below.

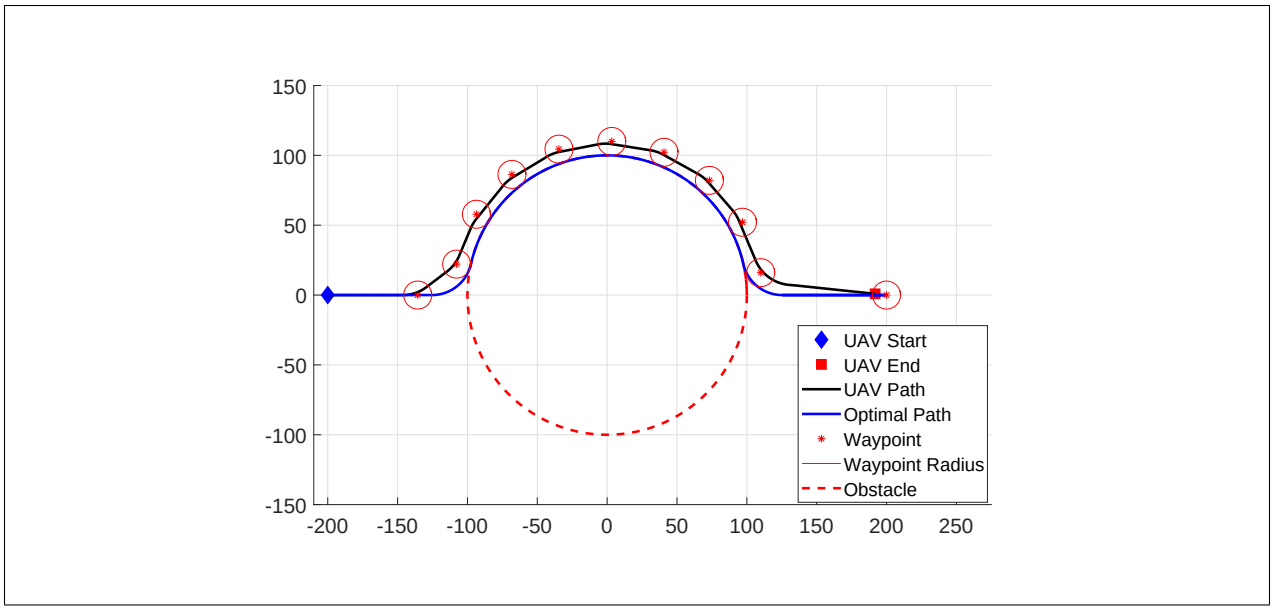

Fig. 2 Simulated Fixed Wing UAV Traversing Waypoints Around Circular Obstacle

It would be beneficial to include obstacle avoidance into a UAVs guidance system to remove the need to communicate with the ground station and path re-planning which may be accomplished with potential field or vector field.

D. Potential Field

Potential field is based on the principle of artificial attractive and repulsive forces acting on a point mass to guide a system to a desired goal while avoiding static and dynamic obstacles [7]. Goals states are represented as an attractive force that pulls a point mass in the direction of minimal energy while obstacles are represented as repulsive forces that act locally to push the point mass away. Potential field is also capable of acting as a path and trajectory planning algorithm [8], possibly eliminating the off-board path planner. An example of potential field can be found in [9–11] which allowed for real time goal seeking with obstacle avoidance on a mobile ground robot equipped with ultrasonic sensors. The robot located at (x_0, y_0) is attracted towards a a goal with constant magnitude force $\overrightarrow{F_t}$ located at (x_t, y_t) and a distance d_t from the robot. In the immediate area of the robot, an active window exists which records integer certainty values inside discrete cells. Cells containing an obstacle provide a repulsive force $\overrightarrow{F_{i,j}}$ opposite in direction to the line-of-sight from vehicle to cell location (x_i, y_j), where (i, j) represents the cell index, F_{cr} is a constant repulsive force, W the vehicle's width, $C_{i,j}$ a cell's certainty, and $d_{i,j}$ the distance to the center of the cell with respect to robots center.

$$\overrightarrow{F_{i,j}} = \frac{F_{cr} W^n C_{i,j}}{d_{i,j}^n} \left(\frac{x_i - x_0}{d_{i,j}} \hat{x} + \frac{y_i - y_0}{d_{i,j}} \hat{y} \right) \tag{8}$$

The total repulsive force exerted on the robot is determined by summing the active cells, shown in Equation 9

$$\overrightarrow{F_r} = \sum_{i,j} \overrightarrow{F_{i,j}} \tag{9}$$

$$\overrightarrow{F_t} = F_{ct} \left(\frac{x_t - x_0}{d_t} \hat{x} + \frac{y_t - y_0}{d_t} \hat{y} \right) \tag{10}$$

Summing together attractive and repulsive forces produce a vector $\overrightarrow{R}$ that can be used for heading guidance, shown in Equation 11.

$$\overrightarrow{R} = \overrightarrow{F_r} + \overrightarrow{F_t} \tag{11}$$

Major drawbacks to potential field were identified in [11] consisting of local minimum and oscillations in corridors. The local minimum problem occurs when closely spaced obstacle's potential combine to produce a well on the descent gradient where a pre-mature stable point is reached. Proposed solutions to local minimum include object clustering and virtual waypoint method [12], virtual escaping route [13], and use of navigation functions [14]. Oscillations in potential field were addressed in [15] and [16].

In addition to local minimum and oscillations, potential field may not be ideal for providing guidance to return to a sensor path after avoiding an obstacle. Once the obstacle has been avoided, the attractive goal will direct the UAV in a straight path which may not lie along the sensor line. Guidance that follows an explicit path, deviates when necessary to avoid obstacles, and return back to the explicit path quickly can be accomplished with path following vector fields.

E. Vector Field Guidance

Vector fields produce continuous heading guidance that asymptotically converges and circulates a path. A comparison between vector field and waypoint guidance techniques was presented in [17] where each method was evaluated based on its complexity, robustness, and accuracy. The vector field model produced guidance that was both robust to external wind disturbances while maintaining a low cross track error. The two most prominent methods for generating vector fields in literature consist of the Lyapunov [18–23] and Goncalves [24–27] method. Lyapunov vector fields for converging and following straight and circular paths were described in [18]. Straight and circular path vector fields can be selectively activated throughout flight to form more complex paths, shown in [18–20, 28]. Lyapunov vector field for curved path following was presented in [23] which may allow for more complex paths and eliminates the need to switch between vector fields.

F. GVF

The Gonvalves Vector Field (GVF) method produces a similar field, however has several advantages over LVFs. GVF produces an n-dimensional vector field that converges and circulates to both static and time varying paths. Additionally, convergence, circulation, and time-varying terms that make up the GVF are decoupled from each other allowing for easy weighting of the total field. GVFs converge and circulate at the intersection, or level set, of $n-1$ dimensional implicit surfaces ($\alpha_i : \mathbb{R}^n \rightarrow \mathbb{R} | i = 1, ..., n-1$). The integral lines of the field are guaranteed to converge and circulate the level set when two conditions are met: 1) the implicit surface functions are positive definite and 2) have bounded derivatives.

The total vector field $\overrightarrow{V}$ is calculated by:

$$\overrightarrow{V} = G\nabla V + H \wedge_{i=1}^{n-1} \nabla\alpha_i - LM(\alpha)^{-1}a(\alpha) \tag{12}$$

or in component form:

$$\overrightarrow{V} = G\overrightarrow{V}_{conv} + H\overrightarrow{V}_{circ} + L\overrightarrow{V}_{tv} \tag{13}$$

where $\overrightarrow{V}_{conv}$ produces vectors perpendicular to the path, $\overrightarrow{V}_{circ}$ produces vectors parallel to the path, and $\overrightarrow{V}_{tv}$ is a feed-forward term that produces vectors accounting for a time varying path. The multiplicative factors G, H, and L are scalar weights to influence the strength of each field component.

Convergence is calculated by:

$$\vec{V}_{conv} = \nabla V \tag{14}$$

where the potential function V is:

$$V = -\sqrt{{\alpha_1}^2 + {\alpha_2}^2} \tag{15}$$

$$\nabla V = \begin{bmatrix} \frac{dV}{dx} \\ \frac{dV}{dy} \\ \frac{dV}{dz} \end{bmatrix} \tag{16}$$

Circulation is calculated by taking the wedge product of the gradients of the surface functions:

$$\vec{V}_{circ} = \wedge_{i=1}^{n-1} \nabla\alpha_i \tag{17}$$

In the case of $(n = 3)$ the wedge product simplifies as the cross product:

$$\vec{V}_{circ} = \nabla\alpha_1 \times \nabla\alpha_2 \tag{18}$$

The feed-forward time-varying component is calculated by:

$$\vec{V}_{tv} = M^{-1} a \tag{19}$$

where,

$$M = \begin{bmatrix} \nabla\alpha_1^T \\ \nabla\alpha_2^T \\ (\nabla\alpha_1 \times \nabla\alpha_2)^T \end{bmatrix} \tag{20}$$

$$a = \begin{bmatrix} \frac{\partial\alpha_1}{\partial t} & \frac{\partial\alpha_2}{\partial t} & 0 \end{bmatrix}^T \tag{21}$$

Intersecting two flat planes $(\alpha_1 = z, \alpha_2 = x)$ produces a GVF that converges and circulates a straight path, shown in Figure 4.

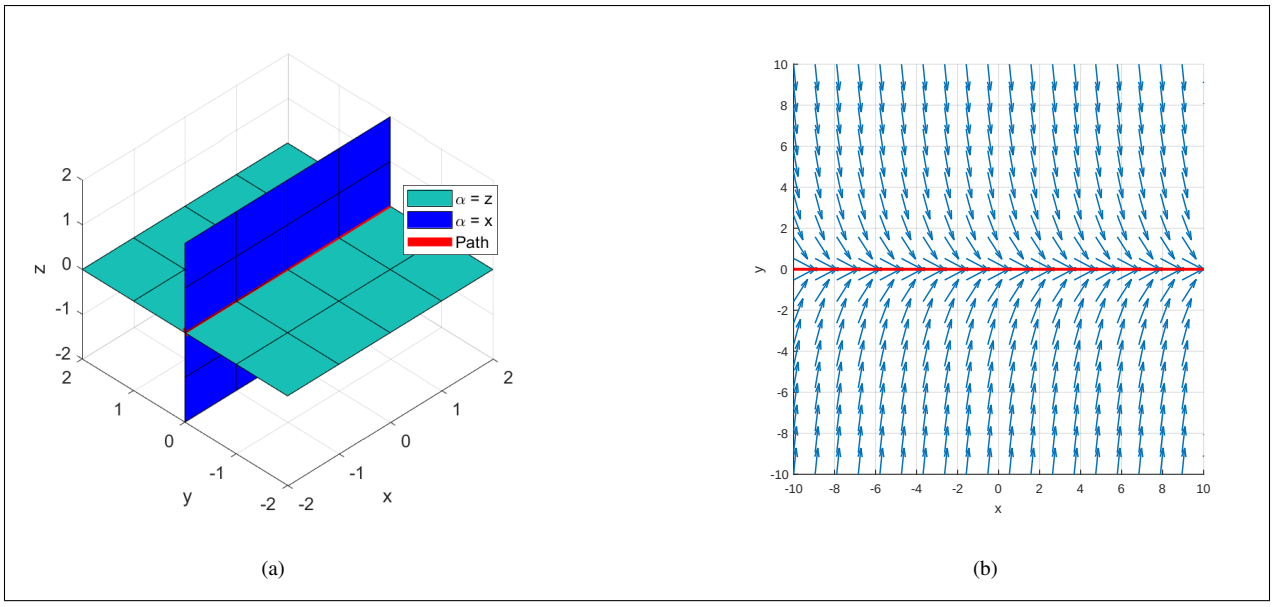

Fig. 3 GVF converging and circulating straight path

A GVF for converging and circulating a circular path can be produced by intersecting a plane and a cylinder $(\alpha_1 = z, \alpha_2 = x^2 + y^2 - r^2)$.

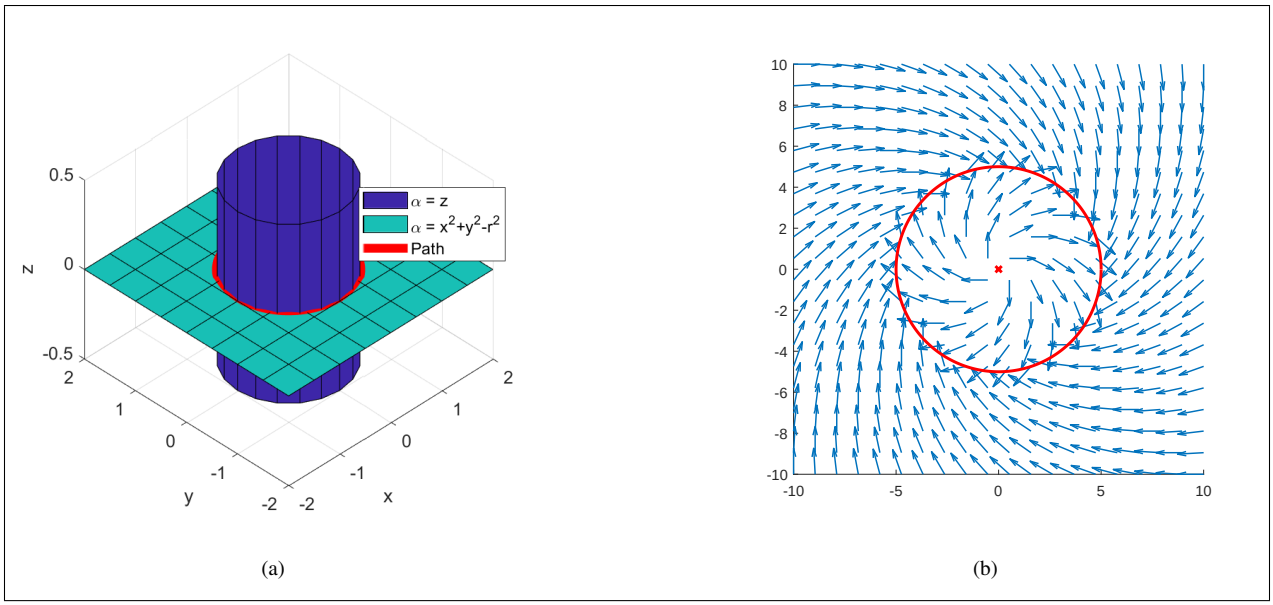

Fig. 4 GVF converging and circulating circular path

GVF was compared against LVF in a standoff tracking scenario in [Wilhelm] where a fixed wing UAV was tasked with with loitering around a moving ground target while avoiding static obstacles. A circular time-varying attractive vector field was attached to a moving ground target. Static circular repulsive vector fields centered at the obstacles and weighted by hyperbolic tangent decay functions were summed with the attractive circular field to produce a target loitering and obstacle avoidance guidance. The performance of Lyapunov [21] and gradient vector field [24–26] were compared for their cross track error with respect to the loiter circle. Gradient vector field had favorable performance due to compensation for a time-varying vector field. The gradient vector field technique also has the benefit of decoupled weighting parameters for convergence, circulation, and time-varying terms, allowing for easy modification of field behavior.

Decay functions for avoidance fields using GVF were also investigated in [Zhu] for obstacles present on a straight path. When summing attractive and repulsive vector fields there is the possibility of guidance singularities, where magnitude and direction are equal and opposite. The presence of singularities were not addressed in [Wilhelm] and [Zhu], mentioned briefly in [18] and observed in [29]. For fixed wing UAVs the lack of guidance may prevent the UAV from avoiding an obstacle, while multi-rotor UAVs may end up in a trap situation. Singularities may be present at any location where a goal field and obstacle field are of equal strength. Detecting singularities and modifying the GVF for an improved obstacle avoidance is now considered.

III. methods

The static weight vector field for straight lines and circular obstacles will be presented. A numerical method for detecting singularities in a summed vector field will be discussed. The modified vector field law with dynamic weights will be presented. Simulations comparing waypoint, potential field, and vector field guidance will be presented for worst case scenario with an obstacle centered on the sensor path. Lastly, a flight test with a multirotor UAV simulating Dubin's constraints of a fixed wing aircraft will be shown.

A. Path Following with GVF

Path following guidance for a planar UAV at position (x, y) for a time invariant line is achieved by summing together convergence $\overrightarrow{V}_{conv}$ and circulation $\overrightarrow{V}_{circ}$ terms shown in Equation 13, where the plane defined by implicit surface function α_1 is at angle δ and plane α_2 is at constant height of $Z = 1$ shown in Equations 22 and 23 respectively.

$$\alpha_1 = cos(\delta)x + sin(\delta)y \tag{22}$$

$$\alpha_2 = z \tag{23}$$

The gradient potential, ∇V is shown in Equation 24.

$$\nabla V = -\frac{1}{2(\sqrt{\cos^2(\delta)x^2 + 2\cos(\delta)\sin(\delta)xy + \sin^2(\delta)y^2})} \begin{bmatrix} 2x\cos^2(\delta) + 2\cos(\delta)\sin(\delta)y \\ 2y\sin^2(\delta) + 2\cos(\delta)\sin(\delta)x \\ 2 \end{bmatrix} \tag{24}$$

Circulation is calculated by the cross product of the surface function gradients, which evaluates to that shown in Equation 25.

$$\vec{V}_{circ} = \begin{bmatrix} sin(\theta) \\ -cos(\theta) \\ 0 \end{bmatrix} \tag{25}$$

Guidance for a path at angle $\delta = 0$ and equal parts circulation and convergence weights $G = H = 1$ is shown in Figure 5 below.

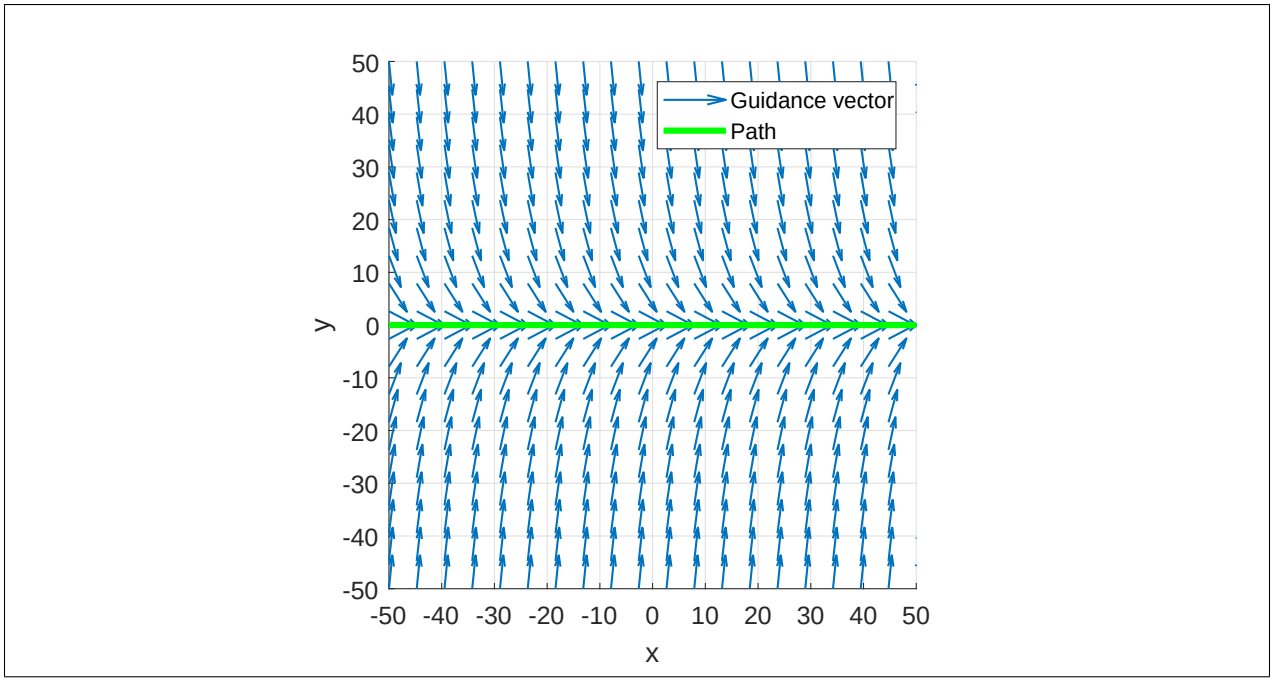

Fig. 5 Straight Path Following Vector Field

B. Avoidance

A circular avoidance vector field centered at (x_c, y_c) is constructed by intersecting a cylinder, Equation 26, and a plane 27.

$$\alpha_1 = (x - x_c)^2 + (y - y_c)^2 - r^2 \tag{26}$$

$$\alpha_2 = z \tag{27}$$

Convergence is determined by the gradient of the potential function 24, which when simplified evaluates to

$$\nabla V = A\vec{B} \tag{28}$$

where

$$A = \frac{-1}{\sqrt{\bar{x}^4 + \bar{y}^4 + 2\bar{x}^2\bar{y}^2 - 2r^2\bar{x}^2 - 2r^2\bar{y}^2 + r^2 + z^2}} \tag{29}$$

$$\overrightarrow{B} = \begin{bmatrix} 2\bar{x}^3 + 2\bar{x}\bar{y}^2 - 2r^2\bar{x} \\ 2\bar{y}^3 + 2\bar{x}^2\bar{y} - 2r^2\bar{y} \\ z \end{bmatrix} \tag{30}$$

and

$$\bar{x} = x - x_c \tag{31}$$

$$\bar{y} = y - y_c \tag{32}$$

Circulation is calculated from the cross product of each implicit surface function's gradient, which simplifies to

$$\overrightarrow{V}_{circ} = \begin{bmatrix} 2(y - y_c) \\ -2(x - x_c) \\ 0 \end{bmatrix} \tag{33}$$

Strictly repulsion guidance is produced by assigning a negative weight to the convergence term G, no circulation $H = 0$, and a small path radius r to prevent trap situations. Limiting the distance at which the field has influence is achieved with a decay function shown in Equation 34 where d is the range to the center of the obstacle and R is the radius where the field has near zero strength.

$$P = -\tanh\left(\frac{2\pi d}{R} - \pi\right) + 1 \tag{34}$$

$$d = \sqrt{\bar{x}^2 + \bar{y}^2} \tag{35}$$

A strictly repulsive field $\overrightarrow{V}_{obst}$ with $G = -1$, $H = 0$, $r = 0.01$, and $R = 35$ is shown in Figure 6.

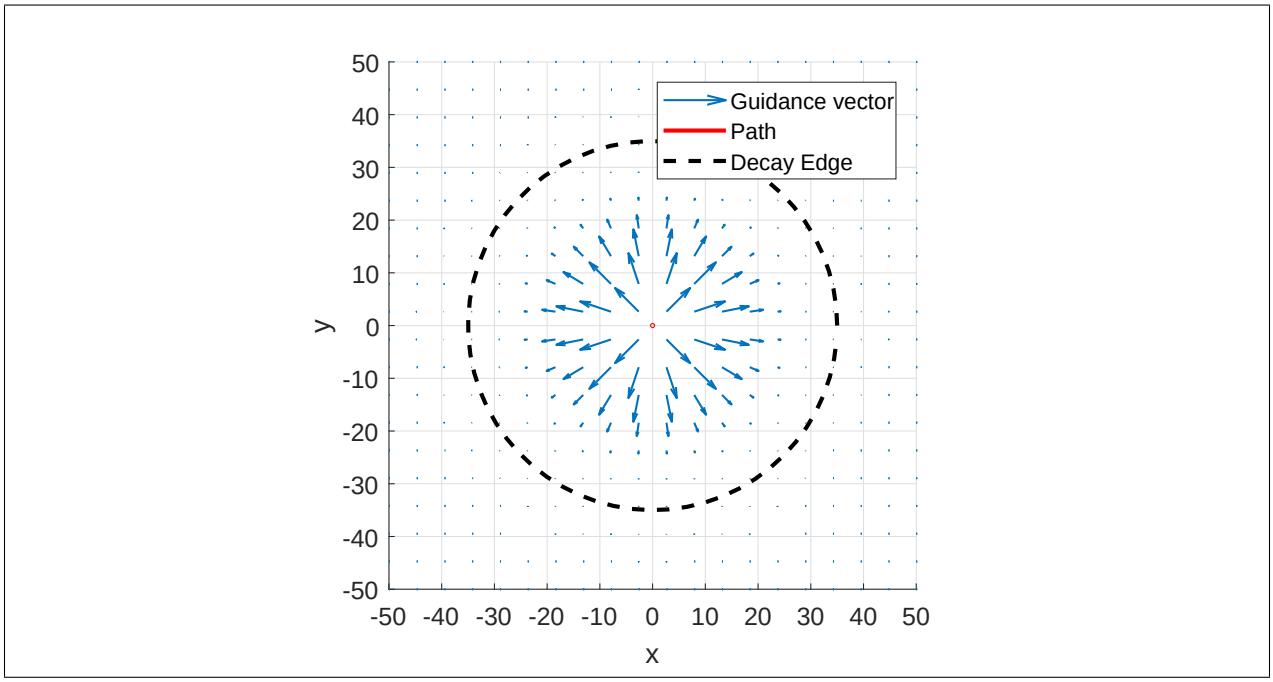

Fig. 6 Repulsive Vector Field with Decay

Summing together the path following field with an obstacle centered on the path results in the guidance $\overrightarrow{V}_G$ shown in Figure 7.

$$\overrightarrow{V}_g = \overrightarrow{V}_{path} + P\overrightarrow{V}_{obst} \tag{36}$$

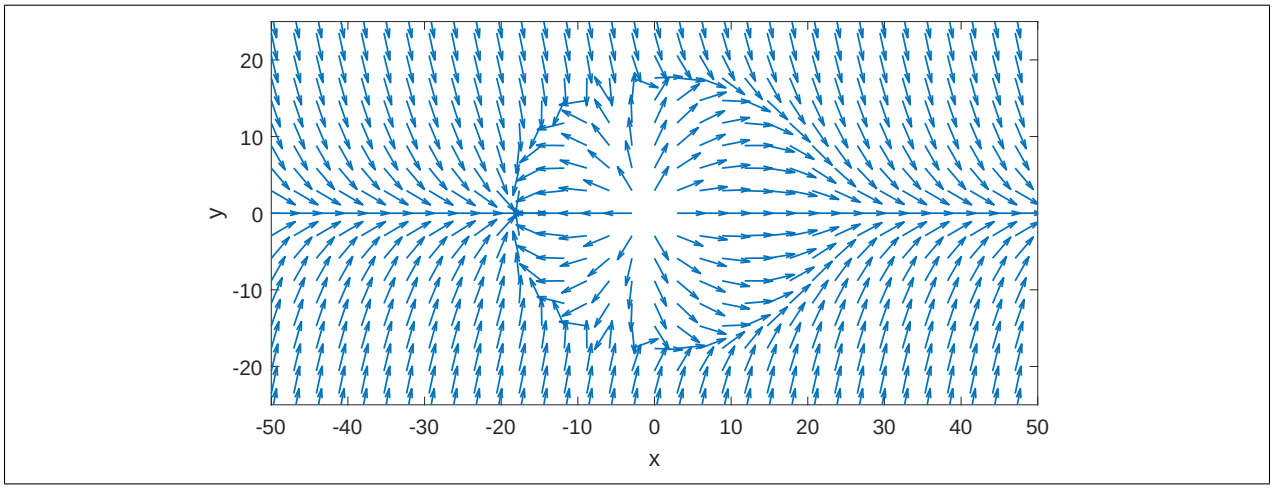

Fig. 7 Summed Vector Field Guidance

The total summed guidance shown in Figure 7 shows the normalized guidance vectors to be used for UAV guidance. Singularities are present in the above guidance due to the repulsive vectors of the obstacle canceling out the path following vectors. Identifying the location of these singularities will now be addressed.

C. Singularity Detection

Singularities are expected to exist where the magnitude of the vector $\overrightarrow{V}_g$ has a magnitude equal to zero, shown in Equation 37. A heatmap of the vector magnitude shows that singularities are present where the fields have equal strength, shown in Figure 8. An analytical solution to Equation 37 may be difficult to obtain, therefore a numerical approach with initial conditions placed at the radius of equal strength, $R/2$, can be used.

$$||\overrightarrow{V}_g|| = 0 \tag{37}$$

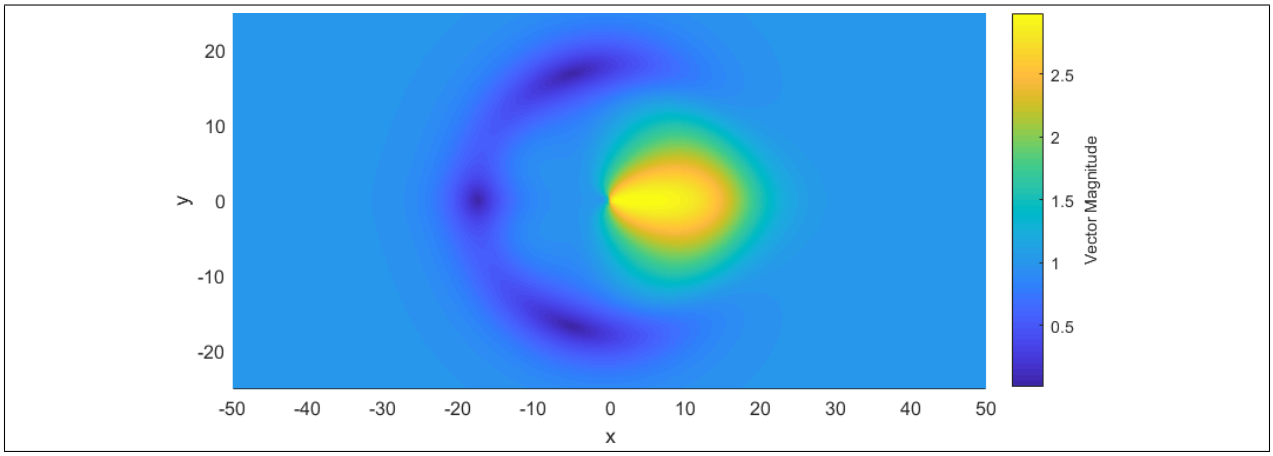

Fig. 8 Summed Vector Field Magnitude Heat Map

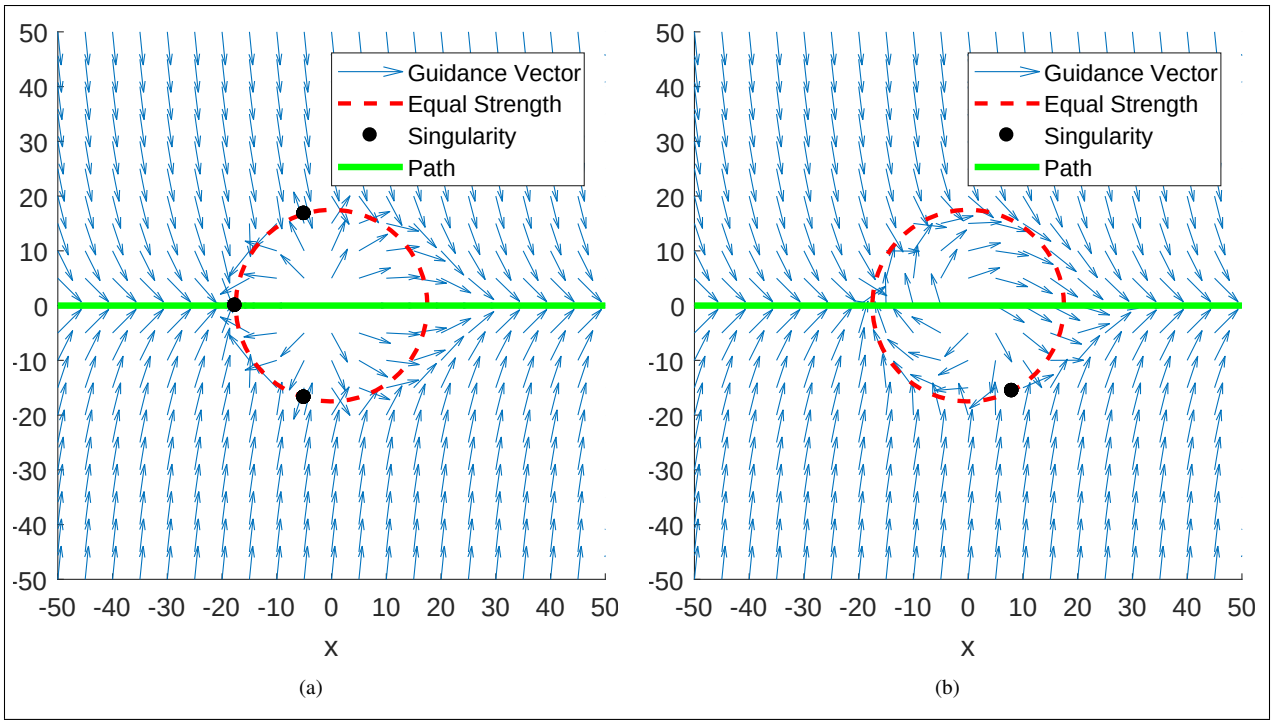

Fig. 9 Singularities Detected in Summed Field

Solving for the location of singularities using a numerical solver with initial conditions placed at the radius of equal strength for the field in 7 is shown in Figure 9a. Modifying the repulsive field with a non-zero circulation weight can reduce the number of singularities as well as remove them for the UAVs path. Additionally, circulation directs the UAV around obstacle in a deterministic way. A circulation weight of $H = 1$ produces the guidance with a singularity removed from the path shown in Figure 9b. Determining the exact values of R and H to produce an avoidance guidance that minimizes deviation from the path will now be discussed.

D. Static Modified Weights

Determining the decay radius R and circulation weight H for a repulsive vector field depends on the UAVs speed u and turnrate $\dot{\theta}$. An obstacle located at a lateral distance Y_0 from the pre-planned sensor path has a radius r_O equal to a scalar multiple of the UAVs turn radius, shown in Equation 38. The multiple n is bounded on the interval $[1, \infty)$.

$$r_O = n\theta_r \tag{38}$$

The repulsive field decay radius R, expressed in k multiples of the obstacles radius is shown in Equation 39 and also bounded on the interval $[1, \infty)$.

$$R = kr_O \tag{39}$$

The decay multiple k and circulation H are then determined by minimizing the cost function 40, where y is the lateral deviation from the path in the I frame and the function j penalizes the UAV for entering the obstacle radius. The sign of H can be determined from the LOS angle between the UAV and the obstacle such that the UAV travels around the obstacle in the correct, least distance, direction.

$$\underset{H,k}{\text{minimize}} \quad \frac{1}{R}\int_{t_f}^{0} y dt + j(x, y) \tag{40}$$

$$j(x, y) = \begin{cases} 100dt & \sqrt{(x - xc)^2 + (y - yc)^2} \leq r_O \\ 0 & \sqrt{(x - xc)^2 + (y - yc)^2} > r_O \end{cases} \tag{41}$$

A UAV with a speed of $u = 20m/s$ and turning rate of $\dot{\theta} = 20deg/s$ following a straight vector field path is shown avoiding an obstacle of radius $n = 2$ in Figure 10 below.

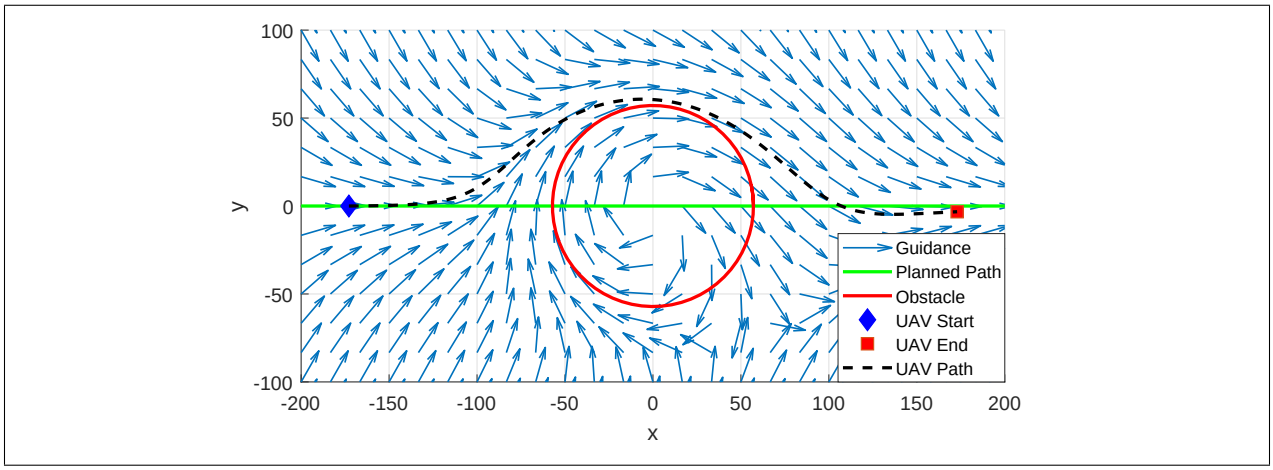

Fig. 10 UAV Avoiding Obstacle with Fixed Repulsive Vector Field

The definition of obstacle and decay field radius in terms of vehicle turn radius θ_r allows for a single decay factor k and circulation H to be applicable for multiple velocities. This generalizes the avoidance field parameter selection problem and allows for a two dimensional lookup table to be generated for a number of obstacle radius factors n and obstacle lateral positions Y_0 for real time obstacle avoidance.

Simply summing together attractive and repulsive fields will always result in the UAV leaving the path pre-maturely, not utilizing its minimum tunrning radius, resulting in sensor path left unobserved. Modifying the vector field weights dynamically increases the path covered and will be discussed next.

E. Modified Path Following Vector Field

The summed guidance results in the UAV leaving the path pre-maturely and slowly returns to the path. Gradually leaving and returning to the path is a result of the slow transition between attractive and repulsive field dominating the guidance. It is desired that the UAV follows the path up until the UAV must turn to avoid the obstacle and quickly return to the path. To accomplish this, a modification to attractive and repulsive fields must take place. Additionally, improved tracking of the outside of the obstacle can be achieved by modifying the convergence strength of the repulsive field. The modified vector field guidance with attractive weight M and repulsive weight N is considered without a decay function P, shown in Equation 42

$$\overrightarrow{V}_g = M\overrightarrow{V}_{path} + N\overrightarrow{V}_{obst} \tag{42}$$

While the UAVs horizontal position x in the I frame is less than the turning distance $\tilde{x}$, the attractive weight $M = 1$ and the repulsive weight is null at $N = 0$. Once the UAVs horizontal position reaches the turning distance, $x = \tilde{x}$ the attractive field weight switches to null $M = 0$ and repulsive weight dominates at $N = 1$. The repulsive field has a constant circulation of unity with sign equal to that of the UAVs lateral position with respect to the I frame. Convergence becomes a function of the UAVs relative heading with respect to the obstacle center β, defined in Equation 43.

$$\beta = \pi - \tan^{-1}\left(\frac{y - Y_0}{x}\right) + \theta \tag{43}$$

The convergence weight becomes:

$$g = -\cos(|\beta|) \tag{44}$$

When the UAV has a heading towards the obstacle center, the repulsion is maximized at -1. As the UAVs heading becomes perpendicular to the LOS to the obstacle center, the repulsion falls off to zero and circulation dominates. If the UAVs heading begins to drift back towards the obstacle, either by wind or another external disturbance, g will decrease

to counteract the deviation. When the UAVs horizontal position $x > \hat{x}$ the repulsive field weight nulls $N = 0$ and the attractive field becomes unity $M = 1$.

The modified VF guidance eliminates the need for a minimizer or lookup table, eliminates singularities since the two fields will never be equal strength, and provides a guidance comparable to waypoint guidance without the need to re-plan a path.

IV. Simulations

A comparision of waypoint, VFF, strictly repulsive GVF, and the modified weighted GVF were compared for both their deviation from the sensor path and how closely the avoidance followed an optimal path around the obstacle. For each guidance method, the UAV is tasked with following a straight sensor path. An obstacle located at $(0, 0)$ must be avoided. Waypoints were generated around the obstacle using the optimal avoidance path with a waypoint radius of 20 meters. The VFF provided a attractive force for the goal of 0.8 while the obstacle provided a repulsive force of -2. With an obstacle width of 5 meters and field exponential of $n = 2$, the VFF avoids the obstacle and gradually returns to the path.

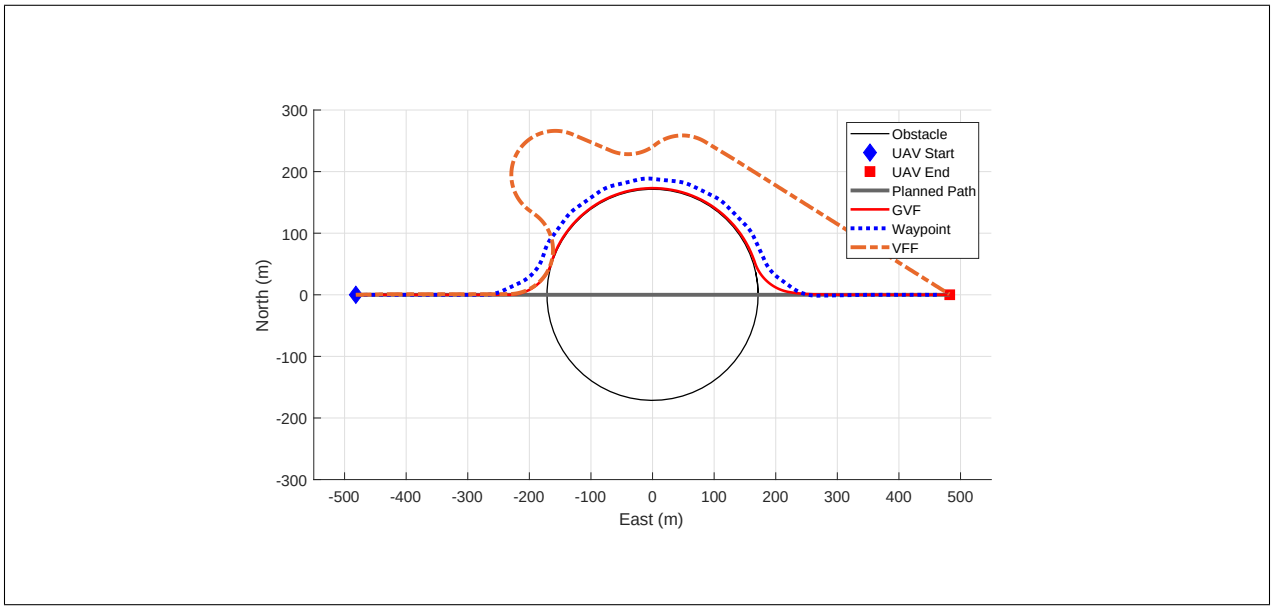

Fig. 11

V. Conclusion

Method	Cost (-)	RMS Error (m)
Waypoint	16.34	16.75
VFF	34.87	91.65
GVF	13.79	1.65

Appendix

Acknowledgments

References

[1] Ariyur, K. B., and Fregene, K. O., "Autonomous tracking of a ground vehicle by a UAV," *American Control Conference, 2008*, IEEE, 2008, pp. 669–671.

[2] Teuliere, C., Eck, L., and Marchand, E., "Chasing a moving target from a flying UAV," *Intelligent Robots and Systems (IROS), 2011 IEEE/RSJ International Conference on*, IEEE, 2011, pp. 4929–4934.

[3] Oh, H., Kim, S., Shin, H.-S., Tsourdos, A., and White, B., "Coordinated standoff tracking of groups of moving targets using multiple UAVs," *Control & Automation (MED), 2013 21st Mediterranean Conference on*, IEEE, 2013, pp. 969–977. URL http://ieeexplore.ieee.org/abstract/document/6608839/.

[4] Hyondong Oh, Seungkeun Kim, Hyo-sang Shin, and Tsourdos, A., "Coordinated standoff tracking of moving target groups using multiple UAVs," *IEEE Transactions on Aerospace and Electronic Systems*, Vol. 51, No. 2, 2015, pp. 1501–1514. doi:10.1109/TAES.2015.140044, URL http://ieeexplore.ieee.org/document/7126199/.

[5] Ulun, S., and Unel, M., "Coordinated motion of UGVs and a UAV," *Industrial Electronics Society, IECON 2013-39th Annual Conference of the IEEE*, IEEE, 2013, pp. 4079–4084. URL http://ieeexplore.ieee.org/abstract/document/6699789/.

[6] Wilhelm, J., Clem, G., and Eberhart, G., "Direct Entry Minimal Path UAV Loitering Path Planning," *Aerospace*, Vol. 4, No. 2, 2017, p. 23. doi:10.3390/aerospace4020023, URL http://www.mdpi.com/2226-4310/4/2/23.

[7] Khatib, O., "Real-time obstacle avoidance for manipulators and mobile robots," *The international journal of robotics research*, Vol. 5, No. 1, 1986, pp. 90–98. URL http://journals.sagepub.com/doi/abs/10.1177/027836498600500106.

[8] Rimon, E., "Exact Robot Navigation Using Artificial Potential Functions.pdf," , 1992.

[9] Borenstein, J., and Koren, Y., "Real-time obstacle avoidance for fast mobile robots in cluttered environments," *Robotics and Automation, 1990. Proceedings., 1990 IEEE International Conference on*, IEEE, 1990, pp. 572–577. URL http://ieeexplore.ieee.org/abstract/document/126042/.

[10] Borenstein, J., and Koren, Y., "The vector field histogram-fast obstacle avoidance for mobile robots," *IEEE transactions on robotics and automation*, Vol. 7, No. 3, 1991, pp. 278–288. URL http://ieeexplore.ieee.org/abstract/document/88137/.

[11] Koren, Y., and Borenstein, J., "Potential Field Methods and their inherent limitions for morbile robot navigation.pdf," , 1991. URL http://ieeexplore.ieee.org/document/131810/.

[12] Liu, Y., and Zhao, Y., "A virtual-waypoint based artificial potential field method for UAV path planning," *Guidance, Navigation and Control Conference (CGNCC), 2016 IEEE Chinese*, IEEE, 2016, pp. 949–953. URL http://ieeexplore.ieee.org/abstract/document/7828913/.

[13] Kim, D. H., "Escaping route method for a trap situation in local path planning," *International Journal of Control, Automation and Systems*, Vol. 7, No. 3, 2009, pp. 495–500. doi:10.1007/s12555-009-0320-7, URL http://link.springer.com/10.1007/s12555-009-0320-7.

[14] Goerzen, C., Kong, Z., and Mettler, B., "A Survey of Motion Planning Algorithms from the Perspective of Autonomous UAV Guidance," *Journal of Intelligent and Robotic Systems*, Vol. 57, No. 1-4, 2010, pp. 65–100. doi:10.1007/s10846-009-9383-1, URL http://link.springer.com/10.1007/s10846-009-9383-1.

[15] Lei Tang, Songyi Dian, Gangxu Gu, Kunli Zhou, Suihe Wang, and Xinghuan Feng, "A novel potential field method for obstacle avoidance and path planning of mobile robot," IEEE, 2010, pp. 633–637. doi:10.1109/ICCSIT.2010.5565069, URL http://ieeexplore.ieee.org/document/5565069/.

[16] Li, G., Yamashita, A., Asama, H., and Tamura, Y., "An efficient improved artificial potential field based regression search method for robot path planning," IEEE, 2012, pp. 1227–1232. doi:10.1109/ICMA.2012.6283526, URL http://ieeexplore.ieee.org/document/6283526/.

[17] Sujit, P., Saripalli, S., and Sousa, J. B., "Unmanned Aerial Vehicle Path Following: A Survey and Analysis of Algorithms for Fixed-Wing Unmanned Aerial Vehicless," *IEEE Control Systems*, Vol. 34, No. 1, 2014, pp. 42–59. doi:10.1109/MCS.2013.2287568, URL http://ieeexplore.ieee.org/document/6712082/.

[18] Nelson, D. R., "Cooperative control of miniature air vehicles," 2005. URL http://scholarsarchive.byu.edu/etd/1095/.

[19] Nelson, D. R., Barber, D. B., McLain, T. W., and Beard, R. W., "Vector field path following for small unmanned air vehicles," *American Control Conference, 2006*, IEEE, 2006, pp. 7–pp. URL http://ieeexplore.ieee.org/abstract/document/1657648/.

[20] Nelson, D., Barber, D., McLain, T., and Beard, R., "Vector Field Path Following for Miniature Air Vehicles," *IEEE Transactions on Robotics*, Vol. 23, No. 3, 2007, pp. 519–529. doi:10.1109/TRO.2007.898976, URL http://ieeexplore.ieee.org/document/4252175/.

[21] Frew, E. W., "Cooperative standoff tracking of uncertain moving targets using active robot networks," *Robotics and Automation, 2007 IEEE International Conference on*, IEEE, 2007, pp. 3277–3282. URL http://ieeexplore.ieee.org/abstract/document/4209596/.

[22] Miao, Z., Thakur, D., Erwin, R. S., Pierre, J., Wang, Y., and Fierro, R., "Orthogonal vector field-based control for a multi-robot system circumnavigating a moving target in 3D," *Decision and Control (CDC), 2016 IEEE 55th Conference on*, IEEE, 2016, pp. 6004–6009. URL http://ieeexplore.ieee.org/abstract/document/7799191/.

[23] Griffiths, S., "Vector Field Approach for Curved Path Following for Miniature Aerial Vehicles," American Institute of Aeronautics and Astronautics, 2006. doi:10.2514/6.2006-6467, URL http://arc.aiaa.org/doi/10.2514/6.2006-6467.

[24] Goncalves, V. M., Pimenta, L. C. A., Maia, C. A., and Pereira, G. A. S., "Artificial vector fields for robot convergence and circulation of time-varying curves in n-dimensional spaces," IEEE, 2009, pp. 2012–2017. doi:10.1109/ACC.2009.5160350, URL http://ieeexplore.ieee.org/document/5160350/.

[25] Gonçalves, V. M., Pimenta, L. C., Maia, C. A., Pereira, G. A., Dutra, B. C., Michael, N., Fink, J., and Kumar, V., "Circulation of curves using vector fields: actual robot experiments in 2D and 3D workspaces," *Robotics and Automation (ICRA), 2010 IEEE International Conference on*, IEEE, 2010, pp. 1136–1141.

[26] Gonçalves, V. M., Pimenta, L. C., Maia, C. A., Dutra, B. C., and Pereira, G. A., "Vector fields for robot navigation along time-varying curves in $ n $-dimensions," *IEEE Transactions on Robotics*, Vol. 26, No. 4, 2010, pp. 647–659. URL http://ieeexplore.ieee.org/abstract/document/5504176/.

[27] Gerlach, A. R., *Autonomous Path-Following by Approximate Inverse Dynamics and Vector Field Prediction*, University of Cincinnati, 2014. URL http://search.proquest.com/openview/432d738d856bf0a9b46acea1b1eee08f/1?pq-origsite=gscholar&cbl=18750&diss=y.

[28] Jung, W., Lim, S., Lee, D., and Bang, H., "Unmanned Aircraft Vector Field Path Following with Arrival Angle Control," *Journal of Intelligent & Robotic Systems*, Vol. 84, No. 1-4, 2016, pp. 311–325. doi:10.1007/s10846-016-0332-5, URL http://link.springer.com/10.1007/s10846-016-0332-5.

[29] Panagou, D., "Motion planning and collision avoidance using navigation vector fields," *Robotics and Automation (ICRA), 2014 IEEE International Conference on*, IEEE, 2014, pp. 2513–2518. URL http://ieeexplore.ieee.org/abstract/document/6907210/.